Exciton spectrum in atomically thin monolayers: The role of hBN encapsulation

Artur O. Slobodeniuk[1,*] and Maciej R. Molas[2,†]

[1]*Department of Condensed Matter Physics, Faculty of Mathematics and Physics, Charles University, CZ-121 16 Prague, Czech Republic*

[2]*Institute of Experimental Physics, Faculty of Physics, University of Warsaw, 02-093 Warsaw, Poland*

(Received 9 January 2023; revised 15 June 2023; accepted 16 June 2023; published 31 July 2023)

The high-quality structures containing semiconducting transition-metal dichalcogenide (S-TMD) monolayers (MLs) required for optical and electrical studies are achieved by their encapsulation in hexagonal BN (hBN) flakes. To examine the effect of hBN thickness in these systems, we consider a model with an S-TMD ML placed between a semi-infinite in the out-of-plane direction substrate and complex top cover layers: a layer of finite thickness, adjacent to the ML, and a semi-infinite in the out-of-plane direction top part. We obtain the expression for the Coulomb potential for such a structure. Using this result, we demonstrate that the energies of excitonic s states in the structure with a WSe_2 ML change significantly for the top hBN with thickness less than 30 layers for different substrate cases, such as hBN and SiO_2. For the larger thickness of the top hBN flake, the binding energies of the excitons are saturated to their values of the bulk hBN limit.

DOI: 10.1103/PhysRevB.108.035427

I. INTRODUCTION

The properties of excitons, i.e., electron-hole (e-h) pairs bounded by Coulomb force, in two-dimensional (2D) monolayers (MLs) of semiconducting transition-metal dichalcogenides (S-TMDs) are remarkably modified due to a significant change in the Coulomb interaction between charge carriers in such 2D crystals [1–3]. The excitons are characterized by the energy spectrum, composed in analogy to the hydrogen series as of the ground ($1s$) and excited ($2s$, $2p$, $3s$, ...) states. Although excitonic states of the s type are observable in the linear optical spectra of S-TMD MLs, i.e., photoluminescence [4–8], transmission [9–11], and reflectance contrast [6,12,13], the excitonic states of the p and d types can be seen in nonlinear experiments performed on S-TMD MLs, i.e., second harmonic generation or two-photon absorption [14–17]. It turns out that the energy spectrum of s-type states in these atomically thin semiconductors does not reproduce the conventional Rydberg series of a 2D hydrogen atom [18,19]. The main reason for that is the dielectric inhomogeneity of the S-TMD structures, i.e., MLs surrounded by dielectric materials. While the Coulomb interaction scales as $\propto 1/\varepsilon r$ with the dielectric response of the surrounding medium ε at large e-h distances r, it appears to be significantly weakened at short e-h distances due to exceptionally strong dielectric screening within the ML plane. Consequently, the energy spectrum of excitons in S-TMD MLs and hence their binding energy, defined as the energy difference between the electronic band gap and the ground $1s$ state, can be strongly modified by the used surrounding media of different dielectric responses.

The influence of the surrounding dielectric on the excitonic ladder has been studied both experimentally and theoretically [6,9–12,20–26]. Note that the theoretical approaches rely mostly on the *ab initio* [27–30], as well as the combination of the *ab initio* and analytical methods [31,32]. In the latter case, the results of *ab initio* simulations have been used as input parameters for the analytical models, which are called quantum electrostatic heterostructure (QEH) models. Such incoming parameters are dielectric functions of the multilayer van der Waals heterostructure [28,31], momentum-dependent matrix elements of the screened Coulomb interaction and the band structure of the valence and conduction bands [30], or even the modified Coulomb potential $V_{3\chi}(\rho)$ in Ref. [32]. However, in all these cases, the calculation of the excitons' energies requires large computational powers. Therefore, the QEH model, which takes into account all the basic characteristics of the heterostructure but requires less computational resources to calculate the excitonic spectrum, is still needed.

Note that the current approach to obtain the highest-quality S-TMD MLs is based on their encapsulation in flakes of atomically flat hexagonal BN (hBN). It results, in particular, in a substantial narrowing of excitonic resonances approaching the homogeneous linewidth limit [33–35], which allows one to precisely identify their spectrum. Consequently, it is of the utmost importance to perform theoretical calculations of the thickness influence of the surrounding media on the excitons spectra in S-TMD MLs within the aforementioned QEH model.

In this work, we investigate theoretically the energy spectrum of free excitons in S-TMD MLs encapsulated in between a semi-infinite in the out-of-plane direction bottom substrate and complex top cover layers consisting of two parts: a layer

*aslobodeniuk@karlov.mff.cuni.cz

†maciej.molas@fuw.edu.pl

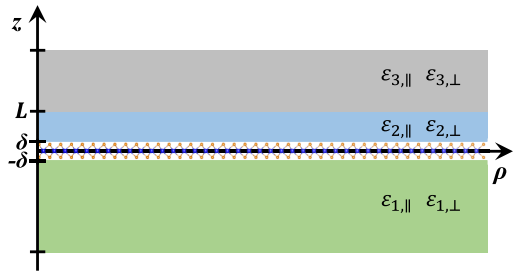

FIG. 1. The schematic illustration of the S-TMD monolayer encapsulated in between a semi-infinite bottom substrate (first layer) and a complex top cover layers consisting of two parts: second layer of the finite thickness, adjacent to the ML and semi-infinite in the out-of-plane direction third part.

of finite thickness L, adjacent to the ML, and semi-infinite in the out-of-plane direction top part with the aid of generalization of the Rytova-Keldysh potential. We demonstrate that the energies of the excitonic s states in such a system with the WSe_2 ML are strongly modified when the thickness of the top hBN layers decreases below about 30 layers. In addition, it results in a significant reduction in excitonic binding energy (E_b) of almost 40% in the transition from the sample without the top hBN layer ($E_b = 256$ meV) to the one with an infinite thickness of the top hBN layer ($E_b = 165$ meV). The similar behavior of the binding energies as a function of the thickness of the top hBN layer has been observed for the other type of substrates.

The paper is organized as follows. In Sec. II, we present the theoretical framework for the calculation of the effective Coulomb potential in a nonhomogeneous planar system, presented in Fig. 1. We analyze the analytical expression for the potential in momentum as well as in coordinate space, as a function of the parameters of the system. In Sec. III, we consider the particular case of the hBN substrate and hBN top flake of finite thickness L, and calculate the corresponding effective Coulomb potential for this case. Using the obtained potential, we calculate in Sec. IV the energy ladder of the excitons for the case of the WSe_2 monolayer as a function of the number of layers of the top hBN flake. In Sec. V, we summarize all the findings. Moreover, the Supplemental Material (SM) [36] presents additional calculations that take into account the discrete structure of the top hBN layer. Using this result, we obtain the spectrum of the excitons in the WSe_2 monolayer with a mono- and bilayer top hBN layer and compare the result found within the model proposed in the main text. We also study the role of the nonzero distance δ between the monolayer and the sub- and superstrate on the excitonic spectrum in such a system.

II. COULOMB POTENTIAL IN THE NONHOMOGENEOUS SYSTEM: GENERAL CASE

Let us consider the S-TMD ML encapsulated in between a semi-infinite bottom substrate (first layer) and complex top cover layers consisting of two parts: second layer of finite thickness $L - \delta$, adjacent to the ML, and semi-infinite in the out-of-plane direction third part. A schematic illustration of the studied system is presented in Fig. 1. The ML is arranged in the xy plane and is centered in the out-of-plane direction ($z = 0$). The bottom substrate, first layer, belongs to the domain $z \in]-\infty, -\delta]$, and is characterized by the in-plane $\varepsilon_{1,\parallel}$ and out-of-plane $\varepsilon_{1,\perp}$ dielectric constants. The top (second) layer, next to the ML, unfolds in the range $z \in [\delta, L]$ with the in-plane $\varepsilon_{2,\parallel}$ and out-of-plane $\varepsilon_{2,\perp}$ dielectric constants. Finally, the third top layer spreads over the distance $z \in [L, \infty[$ and is described by the in-plane $\varepsilon_{3,\parallel}$ and out-of-plane $\varepsilon_{3,\perp}$ dielectric constants.

To find the potential energy between two charges in S-TMD MLs, we solve the following electrostatic problem. We investigate the pointlike charge Q at the point $\mathbf{r} = (\boldsymbol{\rho}, z) = (0, 0, 0)$ and calculate the electric potential in such a system following Refs. [38,39]. Namely, we analyze four regions: bottom ($z \in]-\infty, -\delta]$), ML ($z \in [-\delta, \delta]$), top finite ($z \in [\delta, L]$), and overtop ($z \in [L, \infty[$) media, with potentials $\Phi_1(\boldsymbol{\rho}, z)$, $\Phi(\boldsymbol{\rho}, z)$, $\Phi_2(\boldsymbol{\rho}, z)$, and $\Phi_3(\boldsymbol{\rho}, z)$, respectively. These potentials are defined by the Maxwell equations. It is convenient to present the potentials as a Fourier transform,

$$\Phi_j(\boldsymbol{\rho}, z) = \frac{1}{(2\pi)^2} \int d^2\mathbf{k} e^{i\mathbf{k}\boldsymbol{\rho}} \Phi_j(\mathbf{k}, z), \tag{1}$$

$$\Phi(\boldsymbol{\rho}, z) = \frac{1}{(2\pi)^2} \int d^2\mathbf{k} e^{i\mathbf{k}\boldsymbol{\rho}} \Phi(\mathbf{k}, z). \tag{2}$$

The $\Phi_j(\boldsymbol{\rho}, z)$ potentials for the jth region, where $j = 1, 2, 3$, satisfy Maxwell's equation $\operatorname{div} \mathbf{D}_j(\boldsymbol{\rho}, z) = 0$, which can be written as

$$-\varepsilon_{j,\parallel}\mathbf{k}^2 \Phi_j(\mathbf{k}, z) + \varepsilon_{j,\perp} \frac{d^2\Phi_j(\mathbf{k}, z)}{dz^2} = 0. \tag{3}$$

The solutions of these equations are

$$\Phi_1(\mathbf{k}, z) = B_1 e^{\kappa_1 z} \quad \text{for } z \in]-\infty, -\delta], \tag{4}$$

$$\Phi_2(\mathbf{k}, z) = A_2 e^{-\kappa_2 z} + B_2 e^{\kappa_2 z} \quad \text{for } z \in [\delta, L], \tag{5}$$

$$\Phi_3(\mathbf{k}, z) = A_3 e^{-\kappa_3 z} \quad \text{for } z \in [L, \infty], \tag{6}$$

where $\kappa_j = |\mathbf{k}|\sqrt{\varepsilon_{j,\parallel}/\varepsilon_{j,\perp}} = k\sqrt{\varepsilon_{j,\parallel}/\varepsilon_{j,\perp}}$.

Maxwell's equation in the ML domain, i.e., $z \in [-\delta, \delta]$, reads $\operatorname{div} \mathbf{D}(\boldsymbol{\rho}, z) = 4\pi Q\delta(\boldsymbol{\rho})\delta(z)$. It gives the equation for the potential $\Phi(\mathbf{r}, z)$,

$$\left[\Delta_\parallel + \frac{d^2}{dz^2}\right]\Phi(\boldsymbol{\rho}, z) = -4\pi[Q\delta(\boldsymbol{\rho})\delta(z) - \varrho_{\text{ind}}(\boldsymbol{\rho}, z)], \tag{7}$$

where $\Delta_\parallel$ is the 2D Laplace operator. The first term on the right-hand side of Eq. (7) is the charge density of the charge Q, localized in the ML plane. The second term represents the polarization charge density $\varrho_{\text{ind}}(\boldsymbol{\rho}, z)$, induced in the ML by point charge Q, which is given by

$$\varrho_{\text{ind}}(\boldsymbol{\rho}, z) = \operatorname{div} \mathbf{P}(\boldsymbol{\rho}, z). \tag{8}$$

Following Ref. [38], we present the polarization in the form

$$\mathbf{P}(\boldsymbol{\rho}, z) = \delta(z)\mathbf{P}_\parallel(\boldsymbol{\rho}, z = 0). \tag{9}$$

Using the proportionality between the induced polarization $\mathbf{P}_\parallel(\boldsymbol{\rho}, 0)$ and the in-plane component of the electric field $\mathbf{E}_\parallel(\boldsymbol{\rho}, 0)$, $\mathbf{P}_\parallel(\boldsymbol{\rho}, 0) = \chi_{\text{TMD}}\mathbf{E}_\parallel(\boldsymbol{\rho}, 0)$, we obtain the expression for the induced charge,

$$\varrho_{\text{ind}}(\boldsymbol{\rho}, z) = -\chi_{\text{TMD}}\delta(z)\Delta_\parallel \Phi(\boldsymbol{\rho}, 0). \tag{10}$$

Here, χ_{TMD} is the 2D polarizability of the S-TMD monolayer [38,40]. Introducing the screening length parameter $r_0 = 2\pi\chi_{\mathrm{TMD}}$ and taking the Fourier transformation of Eq. (7) with the induced charge from Eq. (10), one gets

$$\left[\mathbf{k}^2 - \frac{d^2}{dz^2}\right]\Phi(\mathbf{k}, z) = 4\pi Q\delta(z) - 2r_0k^2\delta(z)\Phi(\mathbf{k}, 0). \quad (11)$$

This is a linear nonhomogeneous differential equation of the second order, which solution can be presented as a sum of the general solution of the homogeneous equation and a particular solution of the nonhomogeneous equation (see Ref. [41] and the Supplemental Material [36])

$$\Phi(\mathbf{k}, z) = \Psi e^{-k|z|} + Ae^{-kz} + Be^{kz}. \quad (12)$$

The k-dependent parameters of the potential Ψ, A, and B are not independent. The relations between them are defined from Eq. (7). Integrating it over z in the domain $z \in [-\epsilon, \epsilon]$ and then taking the limit $\epsilon \to 0$, one obtains

$$[1 + r_0k]\Psi + r_0k[A + B] = \frac{2\pi Q}{k}. \quad (13)$$

Using the continuity of the potential and z component of the displacement field $\mathbf{D}(\boldsymbol{\rho}, z)$ on the boundary of two adjusted domains, one obtains the set of equations for the parameters Ψ, A, B, B_1, A_2, B_2, A_3. The boundary conditions for the first and ML domains give the relations

$$B_1e^{-\kappa_1\delta} = \Psi e^{-k\delta} + Ae^{k\delta} + Be^{-k\delta}, \quad (14)$$

$$\varepsilon_1B_1e^{-\kappa_1\delta} = \Psi e^{-k\delta} - Ae^{k\delta} + Be^{-k\delta}. \quad (15)$$

The boundary conditions between the ML and second domains are described by the equations

$$A_2e^{-\kappa_2\delta} + B_2e^{\kappa_2\delta} = \Psi e^{-k\delta} + Ae^{-k\delta} + Be^{k\delta}, \quad (16)$$

$$\varepsilon_2A_2e^{-\kappa_2\delta} - \varepsilon_2B_2e^{\kappa_2\delta} = \Psi e^{-k\delta} + Ae^{-k\delta} - Be^{k\delta}. \quad (17)$$

Finally, the boundary conditions between the second and third domains give

$$A_2e^{-\kappa_2L} + B_2e^{\kappa_2L} = A_3e^{-\kappa_3L}, \quad (18)$$

$$\varepsilon_2A_2e^{-\kappa_2L} - \varepsilon_2B_2e^{\kappa_2L} = \varepsilon_3A_3e^{-\kappa_3L}. \quad (19)$$

Here, we introduce $\varepsilon_j = \sqrt{\varepsilon_{j,\perp}\varepsilon_{j,\parallel}}$ for $j = 1, 2, 3$. Solving these equations together with Eq. (13), we obtain the values of the Ψ, A, and B parameters. Then substituting them into the expression $\Phi(\mathbf{k}, z = 0) = \Psi + A + B = 2\pi Q/k\varepsilon(k)$, we obtain the effective in-plane Coulomb potential $\Phi(\mathbf{k}, z = 0)$. Here, $\varepsilon(k)$ is the dielectric function of the system,

$$\varepsilon(k) = kr_0 + \frac{1 - \left(\frac{\varepsilon_1-1}{\varepsilon_1+1}\right)\left(\frac{\varepsilon_2-1}{\varepsilon_2+1}\right)e^{-4k\delta} - \left(\frac{\varepsilon_2-\varepsilon_3}{\varepsilon_2+\varepsilon_3}\right)\left[\left(\frac{\varepsilon_2-1}{\varepsilon_2+1}\right) - \left(\frac{\varepsilon_1-1}{\varepsilon_1+1}\right)e^{-4k\delta}\right]e^{-2\kappa_2(L-\delta)}}{\left[1 - \left(\frac{\varepsilon_1-1}{\varepsilon_1+1}\right)e^{-2k\delta}\right]\left\{1 - \left(\frac{\varepsilon_2-1}{\varepsilon_2+1}\right)e^{-2k\delta} + \left(\frac{\varepsilon_2-\varepsilon_3}{\varepsilon_2+\varepsilon_3}\right)\left[e^{-2k\delta} - \left(\frac{\varepsilon_2-1}{\varepsilon_2+1}\right)\right]e^{-2\kappa_2(L-\delta)}\right\}}. \quad (20)$$

The coordinate-dependent potential $\Phi(\boldsymbol{\rho})$ for the considered nonhomogeneous system with the dielectric function $\varepsilon(k)$ then reads

$$\Phi(\boldsymbol{\rho}) = Q\int_0^\infty dk\frac{J_0(k\rho)}{\varepsilon(k)}, \quad (21)$$

where $J_0(x)$ is the zeroth Bessel function of the first kind. One can see that the information about the studied heterostructure is fully contained in the second part of the expression. Note that the expression for the in-plane potential contains only the combinations $\varepsilon_j = \sqrt{\varepsilon_{j,\parallel}\varepsilon_{j,\perp}}$ and $\kappa_2 = k\sqrt{\varepsilon_{2,\parallel}/\varepsilon_{2,\perp}}$.

The expression (20) simplifies in two important limits. The limit $L \to \infty$ provides

$$\varepsilon(k) = kr_0 - 1 + \sum_{j=1,2}\frac{1}{1 - \left(\frac{\varepsilon_j-1}{\varepsilon_j+1}\right)e^{-2k\delta}}. \quad (22)$$

This formula interpolates between the case of suspended monolayer $\delta \to \infty$ [$\varepsilon(k) = kr_0 + 1$] and the case of monolayer, encapsulated between two media with dielectric constants $\varepsilon_1, \varepsilon_2$, $\delta \to 0$ [$\varepsilon(k) = kr_0 + [\varepsilon_1 + \varepsilon_2]/2$]. Both limit cases correspond to the so-called Rytova-Keldysh potential in coordinate space, first derived in Refs. [39,42].

Another limit of Eq. (20), which corresponds to the situation with zero distance $\delta \to 0$ between the S-TMD monolayer and the dielectric media, provides

$$\varepsilon(k) = kr_0 + \frac{\varepsilon_1 - \varepsilon_2}{2} + \frac{\varepsilon_2}{1 + \left(\frac{\varepsilon_2-\varepsilon_3}{\varepsilon_2+\varepsilon_3}\right)e^{-2\kappa_2L}}. \quad (23)$$

We consider this dielectric function as the simplest extension of the Rytova-Keldysh model for the case of finite thickness L of the superstrate.

One can see that the key parameter that regulates the shape of $\varepsilon(k)$ is $\tau = \exp(-2\kappa_2L)$. Namely, the long-wavelength $\lambda(k) = 2\pi/k \to \infty$ and short-wavelength $\lambda(k) = 2\pi/k \to 0$ limits correspond to the $\tau \to 1$ and $\tau \to 0$ cases, respectively. In the long-wavelength limit, the dielectric constant is $\varepsilon(k) \to (\varepsilon_1 + \varepsilon_3)/2$. This result reflects the fact that in this case, most of the electric field lines occupy the bottom and second top regions. In this case, neither the S-TMD monolayer nor the thin first top layer contributes significantly to the dielectric response of the system, due to their small volumes in comparison to the volumes of the other regions. The expression for the potential takes the form $\Phi(\mathbf{k}, z = 0) \to 2\pi Q/(k[\varepsilon_1 + \varepsilon_3]/2)$. It provides the following large distance, $\rho \to \infty$, the behavior of the potential in the coordinate space $\Phi(\rho, z = 0) \to Q/(\rho[\varepsilon_1 + \varepsilon_3]/2)$, which is simply the Coulomb potential of point charge Q placed in between two substrates with dielectric constants ε_1 and ε_3, respectively.

In the opposite limit, $\lambda(k) \to 0$, the significant part of the electric lines of the charge occupies the monolayer, the first top layer, and bottom regions. In this case, the effective dielectric constant takes the form $\varepsilon(k) \to kr_0 + (\varepsilon_1 + \varepsilon_2)/2$. As one can see, the second top substrate does not give a contribution to the potential. The corresponding limit defines the small distance, $\rho \to 0$, behavior of the potential $\Phi(\rho, z = 0) \to (\pi Q/2)\{H_0(\rho[\varepsilon_1 + \varepsilon_2]/2r_0) - Y_0(\rho[\varepsilon_1 + \varepsilon_2]/2r_0)\}$.

Finally, note that both coordinate-dependent potentials also correspond to two limits $L \to 0$ and $L \to \infty$ of the thickness

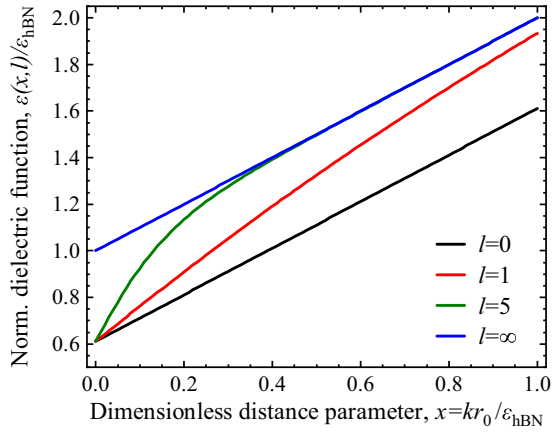

FIG. 2. Normalized dielectric function $\varepsilon(x, l)/\varepsilon_{\mathrm{hBN}}$ for four values of dimensionless length parameter l: $l = 0$, $l = 1$, $l = 5$, and $l = \infty$ (black, red, green, and blue curves, respectively) as a function of a dimensionless distance parameter, $x = kr_0/\varepsilon_{\mathrm{hBN}}$.

L of the first top layer. Therefore, the potential with a finite value of L interpolates between these two potentials, as is depicted in Fig. 3 for particular cases of dielectric constants of the surrounding media.

III. THE COULOMB POTENTIAL IN S-TMD SAMPLE: EFFECT OF FINITE THICKNESS OF hBN top layer

We examine the particular case of an S-TMD ML encapsulated in hBN layers, i.e., $\varepsilon_{1,\parallel} = \varepsilon_{2,\parallel} = \varepsilon_{\mathrm{hBN},\parallel}$, $\varepsilon_{1,\perp} = \varepsilon_{2,\perp} = \varepsilon_{\mathrm{hBN},\perp}$, $\varepsilon_{3,\parallel} = \varepsilon_{3,\perp} = 1$. Following the values available in the literature, we use $\varepsilon_1 = \varepsilon_2 = \varepsilon_{\mathrm{hBN}} = 4.5$ and $\kappa_2 = k\sqrt{\varepsilon_{\mathrm{hBN},\parallel}/\varepsilon_{\mathrm{hBN},\perp}} \approx 1.098\,k$ [9]. Here we use the high-frequency (infrared) values for the dielectric constants of hBN. This is because the typical frequency scale at which the hBN flake responds to the excitons in the WSe_2 monolayer is given approximately by their binding energies of hundreds of meV; see more details in Refs. [9,20,43]. Note that $\varepsilon_{3,\parallel} = \varepsilon_{3,\perp} = 1$ resemble typical experimental conditions, i.e., the sample is placed in air, vacuum, or gaseous helium.

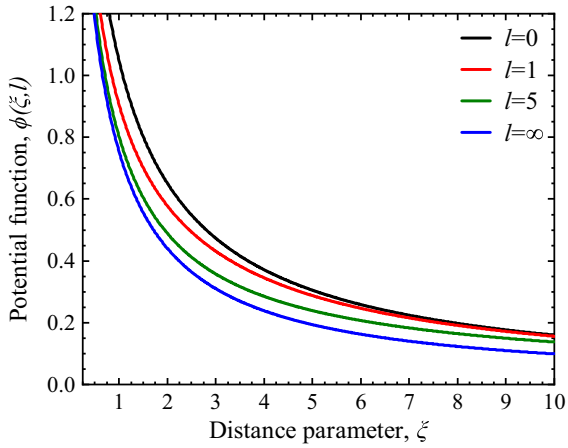

FIG. 3. Potential function $\phi(\xi, l)$ for four values of dimensionless length parameter l: $l = 0$, $l = 1$, $l = 5$, and $l = \infty$ as a function of a dimensionless distance parameter ξ.

Introducing the dimensionless momentum $x = kr_0/\varepsilon_{\mathrm{hBN}}$ and length $l = \varepsilon_{\mathrm{hBN}}L/r_0$ parameters, we obtain the following expression for the effective dielectric constant:

$$\varepsilon(x, l) = \varepsilon_{\mathrm{hBN}}x + \frac{\varepsilon_{\mathrm{hBN}}}{1 + \frac{\varepsilon_{\mathrm{hBN}}-1}{\varepsilon_{\mathrm{hBN}}+1}\exp\left(-2\sqrt{\frac{\varepsilon_{\mathrm{hBN},\parallel}}{\varepsilon_{\mathrm{hBN},\perp}}}xl\right)}. \quad (24)$$

This dielectric function, normalized for $\varepsilon_{\mathrm{hBN}}$, for different values of the dimensionless thickness l of the top hBN flake is presented in Fig. 2.

The corresponding effective potential for the considered case $\Phi(\xi) = (Q/r_0)\phi(\xi, l)$, as a function of the dimensionless distance $\xi = \rho\varepsilon_{\mathrm{hBN}}/r_0$, reads

$$\phi(\xi, l) = \int_0^\infty dx \frac{J_0(x\xi)\left[1 + \frac{\varepsilon_{\mathrm{hBN}}-1}{\varepsilon_{\mathrm{hBN}}+1}\exp\left(-2\sqrt{\frac{\varepsilon_{\mathrm{hBN},\parallel}}{\varepsilon_{\mathrm{hBN},\perp}}}xl\right)\right]}{1 + x\left[1 + \frac{\varepsilon_{\mathrm{hBN}}-1}{\varepsilon_{\mathrm{hBN}}+1}\exp\left(-2\sqrt{\frac{\varepsilon_{\mathrm{hBN},\parallel}}{\varepsilon_{\mathrm{hBN},\perp}}}xl\right)\right]}. \quad (25)$$

Note that in the limit $l \to \infty$, i.e., an ML encapsulated in semi-infinite hBN layers, the potential expression is simplified and gives the well-known Rytova-Keldysh potential [39,42],

$$\phi(\xi, \infty) = \int_0^\infty dx \frac{J_0(x\xi)}{1 + x} = \frac{\pi}{2}[\mathrm{H}_0(\xi) - Y_0(\xi)]. \quad (26)$$

The other limit $l \to 0$ corresponds to the case of an ML deposited on a semi-infinite hBN substrate, uncovered from the top. The related potential also has the Rytova-Keldysh form

$$\phi(\xi, 0) = \frac{\pi}{2}\left[\mathrm{H}_0\left(\frac{\varepsilon_{\mathrm{hBN}} + 1}{2\varepsilon_{\mathrm{hBN}}}\xi\right) - Y_0\left(\frac{\varepsilon_{\mathrm{hBN}} + 1}{2\varepsilon_{\mathrm{hBN}}}\xi\right)\right]. \quad (27)$$

The evolution of the $\phi(\xi, l)$ potential as a function of a ξ parameter is presented in Fig. 3 for four l values. As can be seen in the figure, the strongest $\phi(\xi, l)$ potential is apparent for $l = 0$, while the weakest potential is for the case $l = \infty$, and the potential for $l > 0$ lies in the region in between two former potentials. The obtained results are in full agreement with the previously reported results [9,21,26], where it was shown that an increase in the average dielectric constant of the media surrounding the ML leads to a decrease in the confining potential.

IV. EXCITONIC SPECTRUM IN NONHOMOGENEOUS SYSTEM

Using the $\phi(\xi, l)$ potential, expressed by Eq. (25), we can evaluate the energy spectrum of the excitons in the investigated structure composed of S-TMD ML as a function of the parameter l. The corresponding equation for the eigenvalues is given by

$$\left[b^2\frac{1}{\xi}\frac{d}{d\xi}\left(\xi\frac{d}{d\xi}\right) + 2b\phi(\xi, l) + \epsilon\right]\psi(\xi) = 0, \quad (28)$$

where we introduced $b = \hbar^2\varepsilon_{\mathrm{hBN}}^2/(\mu e^2 r_0)$ and $E = \mathrm{Ry}^*\epsilon$. $\mathrm{Ry}^* = \mu e^4/(2\hbar^2\varepsilon_{\mathrm{hBN}}^2)$ is an effective Rydberg energy and $\psi(\xi)$ represents the wave function of an exciton. $\mu = m_e m_h/(m_e + m_h)$ is the reduced mass of the exciton (e-h pair) with the effective electron (m_e) and hole (m_h) masses and e represents the electron's charge.

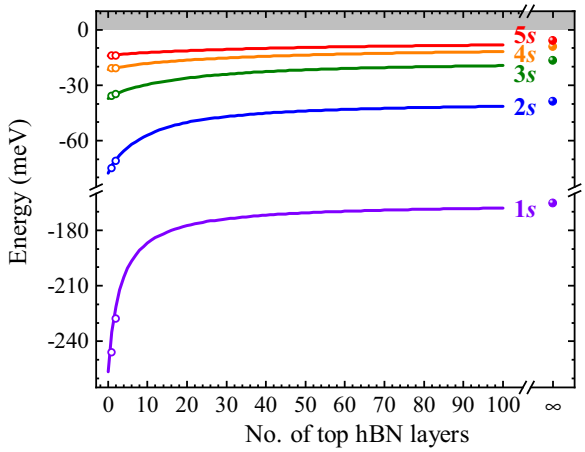

FIG. 4. Energy spectrum of s excitonic state in the WSe_2 ML encapsulated in hBN layers as a function of the thickness of the top hBN layer. The full points correspond to the case of a semi-infinite thickness of top hBN. The colored open points represent the energy spectrum of excitons calculated individually for the mono- and bilayer top hBN (see SM [36] for details). Note that the thickness of the bottom hBN layer is semi-infinite in both cases. The gray-shaded region represents the infinity of states above the band-gap energy.

Let us examine the case of WSe_2 ML with $r_0 = 4.5$ nm [40] and $\mu = 0.21\, m_0$ [6], where m_0 is the electron's mass. It gives $b \approx 1.13357$ and $\mathrm{Ry}^* \approx 141$ meV. For the WSe_2 ML $r_0 = 4.5$ nm, the dimensionless parameter l corresponds to the l nm of the thickness of the top flake of hBN. Taking into account that the distance between the layers in hBN (in other words, the thickness of hBN ML) is $d = 0.33$ nm [44], we conclude that $l = 1$ corresponds to three layers of hBN.

Note that in the case of the few-layer top hBN flake, when its discreteness can play an important role, the phenomenological continuous model of the hBN medium considered here should be additionally verified. To do it, we separately perform the numerical analysis for the ML and bilayer (BL) of the top hBN in the Supplemental Material (SM) [36].

The calculated energy spectra of an exciton for the ground ($1s$) and four excited ($2s$ – $5s$) states as a function of the thickness of the top hBN layer for the aforementioned continuous model as well as the discrete one for the thinnest layers are presented in Fig. 4. Due to the observed evolutions in the figure, three main points can be raised: (i) The continuous model provides a very good method for calculating the exciton spectrum, even in the case of the extremely thin top hBN flake of about 1–2 layers; the largest discrepancy is observed between the homogeneous model and the ML of top hBN for the energy of $1s$ state of about 5%. (ii) The energies of the excitonic states are subjected to the most significant variations for the thinnest top hBN layers with thicknesses below about 30 layers. For thicker top hBN layers, the corresponding excitonic energies are almost fixed. (iii) The thickness effect of the top hBN layer is the largest for the ground $1s$ state of the exciton with its substantial reduction when the number of excitonic states is increased. The maximum change of the $1s$ energy is about 91 meV between two limits: without the top hBN layer and with its infinite thickness. The analogous differences of the $2s$, $3s$, $4s$, and $5s$ states are of the order of 39, 20, 13, and 8 meV, respectively. We can focus on analyzing the excitonic binding energy (E_b, defined as the energy difference between the electronic bang gap and the ground $1s$ state). The dependence of the E_b energy in the WSe_2 ML encapsulated in the hBN layers for selected numbers of the top hBN layer is summarized in Table I. The experimentally measured binding energies of excitons in WSe_2 MLs encapsulated in hBN flakes are about 170 meV [5–7,9]. Although the structures with the hBN encapsulation investigated experimentally differ from the one analyzed in this work, e.g., a WSe_2 ML sandwiched between 10-nm-thick hBN deposited on the core of a single-mode optical fiber [9], the theoretically calculated binding energies are in very good agreement with the experimental ones. Using our approach, the excitonic binding energy can be changed by almost 40% in the transition from the sample without the top hBN layer ($E_b = 256$ meV) to the one with the infinite thickness of the top hBN layer ($E_b = 165$ meV). This reveals that the thickness of the surrounding media of S-TMD MLs also plays a crucial role in the modification of the exciton energy spectrum in S-TMD MLs in addition to the engineering of the surrounding dielectric environment, i.e., the encapsulation of an ML in media characterized by dielectric constants [21].

TABLE I. Calculated binding energies of excitons (E_b) in WSe_2 ML encapsulated in hBN layers for selected numbers of the top hBN layer.

No. top hBN layers	0	3	6	10	20	40	100	∞
E_b (meV)	256	212	197	187	177	172	168	165

To fulfill our results, we consider two additional cases which can be realized in the experiment: (i) the case of the SiO_2 substrate, i.e., $\varepsilon_1 = 2.1$; (ii) the case of the suspended S-TMD monolayer together with the thick hBN flake, i.e., $\varepsilon_1 = 1$. We repeat the calculation of the exciton spectrum in the S-TMD monolayer for both cases and compare them with the previous results in the SM [36]. Finally, we study the general case, presented by Eq. (20), with a nonzero distance gap δ between the S-TMD monolayer and the sub- and superstrate; see SM [36] for details.

V. SUMMARY

We obtained the generalization of the Rytova-Keldysh potential for the heterostructures which consists of the substrate, the monolayer S-TMD, the top hBN flake of finite thickness, and the overtop superstrate. Using the analytical interpretation of the potential, we calculated the energy spectrum of the excitonic states in the S-TMD monolayer placed on a semi-infinite hBN substrate and covered with a top hBN layer with thickness L. We presented that the binding energies of the excitons can be significantly modified due to screening effects and as a function of thickness L. For a WSe_2 ML in such a structure, we demonstrated that the energies of the excitonic states are substantially adjusted for the thinnest top hBN layers with thicknesses below about 30 layers. For the thickness of the top layer larger than 30 layers, the binding

energies of the excitons saturate to the exciton energies in the bulk hBN case.

Additionally, we have found that the thickness effect of the top hBN layer is the largest for the ground 1*s* state of the exciton. It results in a significant reduction in excitonic binding energy that can be changed by almost 40% in the transition from the sample without the top hBN layer to the one with an infinite thickness of the top hBN layer. The proposed model may be applicable to other 2D layered materials in which the screening effects on the excitonic spectrum play an essential role, e.g., 2D perovskites [45].

ACKNOWLEDGMENTS

The work has been supported by the National Science Centre, Poland (Grant No. 2018/31/B/ST3/02111) and by the Czech Science Foundation (Project No. GA23-06369S).

[1] T. Cheiwchanchamnangij and W. R. L. Lambrecht, Phys. Rev. B **85**, 205302 (2012).
[2] A. Ramasubramaniam, Phys. Rev. B **86**, 115409 (2012).
[3] D. Y. Qiu, F. H. da Jornada, and S. G. Louie, Phys. Rev. Lett. **111**, 216805 (2013).
[4] E. Liu, J. van Baren, T. Taniguchi, K. Watanabe, Y.-C. Chang, and C. H. Lui, Phys. Rev. B **99**, 205420 (2019).
[5] S.-Y. Chen, Z. Lu, T. Goldstein, J. Tong, A. Chaves, J. Kunstmann, L. S. R. Cavalcante, T. Woźniak, G. Seifert, D. R. Reichman, T. Taniguchi, K. Watanabe, D. Smirnov, and J. Yan, Nano Lett. **19**, 2464 (2019).
[6] M. R. Molas, A. O. Slobodeniuk, K. Nogajewski, M. Bartos, L. Bala, A. Babiński, K. Watanabe, T. Taniguchi, C. Faugeras, and M. Potemski, Phys. Rev. Lett. **123**, 136801 (2019).
[7] P. Kapuściński, A. Delhomme, D. Vaclavkova, A. O. Slobodeniuk, M. Grzeszczyk, M. Bartos, K. Watanabe, T. Taniguchi, C. Faugeras, and M. Potemski, Commun. Phys. **4**, 186 (2021).
[8] J. C. Sell, J. R. Vannucci, D. G. Suárez-Forero, B. Cao, D. W. Session, H.-J. Chuang, K. M. McCreary, M. R. Rosenberger, B. T. Jonker, S. Mittal, and M. Hafezi, Phys. Rev. B **106**, L081409 (2022).
[9] A. V. Stier, N. P. Wilson, K. A. Velizhanin, J. Kono, X. Xu, and S. A. Crooker, Phys. Rev. Lett. **120**, 057405 (2018).
[10] M. Goryca, J. Li, A. V. Stier, T. Taniguchi, K. Watanabe, E. Courtade, S. Shree, C. Robert, B. Urbaszek, X. Marie, and S. A. Crooker, Nat. Commun. **10**, 4172 (2019).
[11] A. Arora, T. Deilmann, T. Reichenauer, J. Kern, S. M. de Vasconcellos, M. Rohlfing, and R. Bratschitsch, Phys. Rev. Lett. **123**, 167401 (2019).
[12] A. Chernikov, T. C. Berkelbach, H. M. Hill, A. Rigosi, Y. Li, B. Aslan, D. R. Reichman, M. S. Hybertsen, and T. F. Heinz, Phys. Rev. Lett. **113**, 076802 (2014).
[13] I. C. Gerber, E. Courtade, S. Shree, C. Robert, T. Taniguchi, K. Watanabe, A. Balocchi, P. Renucci, D. Lagarde, X. Marie, and B. Urbaszek, Phys. Rev. B **99**, 035443 (2019).
[14] Z. Ye, T. Cao, K. O'Brien, H. Zhu, X. Yin, Y. Wang, S. G. Louie, and X. Zhang, Nature (London) **513**, 214 (2014).
[15] K. He, N. Kumar, L. Zhao, Z. Wang, K. F. Mak, H. Zhao, and J. Shan, Phys. Rev. Lett. **113**, 026803 (2014).
[16] G. Wang, X. Marie, I. Gerber, T. Amand, D. Lagarde, L. Bouet, M. Vidal, A. Balocchi, and B. Urbaszek, Phys. Rev. Lett. **114**, 097403 (2015).
[17] S. Kusaba, Y. Katagiri, K. Watanabe, T. Taniguchi, K. Yanagi, N. Naka, and K. Tanaka, Opt. Express **29**, 24629 (2021).
[18] A. H. MacDonald and D. S. Ritchie, Phys. Rev. B **33**, 8336 (1986).
[19] E. S. Koteles and J. Y. Chi, Phys. Rev. B **37**, 6332 (1988).
[20] A. V. Stier, N. P. Wilson, G. Clark, X. Xu, and S. A. Crooker, Nano Lett. **16**, 7054 (2016).
[21] A. Raja, A. Chaves, J. Yu, G. Arefe, H. M. Hill, A. F. Rigosi, T. C. Berkelbach, P. Nagler, C. Schüller, T. Korn, C. Nuckolls, J. Hone, L. E. Brus, T. F. Heinz, D. R. Reichman, and A. Chernikov, Nat. Commun. **8**, 15251 (2017).
[22] W.-T. Hsu, J. Quan, C.-Y. Wang, L.-S. Lu, M. Campbell, W.-H. Chang, L.-J. Li, X. Li, and C.-K. Shih, 2D Mater. **6**, 025028 (2019).
[23] A. C. Riis-Jensen, M. N. Gjerding, S. Russo, and K. S. Thygesen, Phys. Rev. B **102**, 201402(R) (2020).
[24] M. Bieniek, K. Sadecka, L. Szulakowska, and P. Hawrylak, Nanomaterials **12**, 1582 (2022).
[25] J. Shi, Z. Lin, Z. Zhu, J. Zhou, G. Q. Xu, and Q.-H. Xu, ACS Nano **16**, 15862 (2022).
[26] H. T. Nguyen-Truong, Phys. Rev. B **105**, L201407 (2022).
[27] I. C. Gerber and X. Marie, Phys. Rev. B **98**, 245126 (2018).
[28] S. Latini, T. Olsen, and K. S. Thygesen, Phys. Rev. B **92**, 245123 (2015).
[29] M. Rösner, C. Steinke, M. Lorke, C. Gies, F. Jahnke, and T. O. Wehling, Nano Lett. **16**, 2322 (2016).
[30] M. Florian, M. Hartmann, A. Steinhoff, J. Klein, A. W. Holleitner, J. J. Finley, T. O. Wehling, M. Kaniber, and C. Gies, Nano Lett. **18**, 2725 (2018).
[31] K. Andersen, S. Latini, and K. S. Thygesen, Nano Lett. **15**, 4616 (2015).
[32] D. Van Tuan, M. Yang, and H. Dery, Phys. Rev. B **98**, 125308 (2018).
[33] O. A. Ajayi, J. V. Ardelean, G. D. Shepard, J. Wang, A. Antony, T. Taniguchi, K. Watanabe, T. F. Heinz, S. Strauf, X.-Y. Zhu, and J. C. Hone, 2D Mater. **4**, 031011 (2017).
[34] F. Cadiz, E. Courtade, C. Robert, G. Wang, Y. Shen, H. Cai, T. Taniguchi, K. Watanabe, H. Carrere, D. Lagarde, M. Manca, T. Amand, P. Renucci, S. Tongay, X. Marie, and B. Urbaszek, Phys. Rev. X **7**, 021026 (2017).
[35] J. Wierzbowski, J. Klein, F. Sigger, C. Straubinger, M. Kremser, T. Taniguchi, K. Watanabe, U. Wurstbauer, A. W. Holleitner, M. Kaniber, K. Müller, and J. J. Finley, Sci. Rep. **7**, 12383 (2017).
[36] See Supplemental Material at http://link.aps.org/supplemental/10.1103/PhysRevB.108.035427 for additional calculations that take into account the discrete structure of the top hBN layer and the role of the nonzero distance δ between the monolayer and the sub- and superstrate on the excitonic spectrum, which includes Refs. [6,20,30,37,38,40,41].
[37] A. Laturia, M. L. Van de Put, and W. G. Vandenberghe, npj 2D Mater. Applic. **2**, 6 (2018).
[38] P. Cudazzo, I. V. Tokatly, and A. Rubio, Phys. Rev. B **84**, 085406 (2011).

[39] L. V. Keldysh, Pis'ma Zh. Eksp. Teor. Fiz. **29**, 716 (1979) [JETP Lett. **29**, 658 (1979)].

[40] T. C. Berkelbach, M. S. Hybertsen, and D. R. Reichman, Phys. Rev. B **88**, 045318 (2013).

[41] L. Kipczak, A. O. Slobodeniuk, T. Woźniak, M. Bhatnagar, N. Zawadzka, K. Olkowska-Pucko, M. Grzeszczyk, K. Watanabe, T. Taniguchi, A. Babiński, and M. R. Molas, 2D Mater. **10**, 025014 (2023).

[42] N. S. Rytova, Moscow Univ. Phys. Bull. **3**, 30 (1967).

[43] A. Steinhoff, T. O. Wehling, and M. Rösner, Phys. Rev. B **98**, 045304 (2018).

[44] B. Xu, M. Lv, X. Fan, W. Zhang, Y. Xu, and T. Zhai, Integrat. Ferroelectr. **162**, 85 (2015).

[45] M. Baranowski and P. Plochocka, Adv. Energy Mater. **10**, 1903659 (2020).